Structural Changes in Polyester Fibers during Fatigue

Ch. OUDET and A. R. BUNSELL, *Ecole des Mines de Paris, Centre des Matériaux, B.P. 87, 91003 Evry Cédex, France,* and R. HAGEGE and M. SOTTON, *Institut Textile de France, 35 Rue des Abondances, B.P. 79, 92105 Boulogne Billancourt Cédex, France*

Synopsis

Structural changes occurring during the fatigue failure of polyester fibers have been identified, and a comparison has been made with untested fibers and fibers which were subjected to cyclic loading conditions which did not produce fatigue. Fatigue failure was seen to result in a distinctive fracture morphology. Infrared spectrometry and X-ray diffraction revealed a lowering of crystallinity under fatigue conditions but not under other loading conditions. Transmission electron microscopy and electron diffraction revealed the creation of amorphous zones which are supposed as coalescing to form an amorphous band seen along and ahead of the fatigue crack. The zone just ahead of the fatigue crack tip is shown to contain voids. Crack propagation involves, therefore, the joining up of these voids and development along the amorphous band.

INTRODUCTION

Certain organic synthetic fibers, including polyamide and poly(ethylene terephthalate) (PET), are known to fail by a distinct fatigue process when subjected to certain tensile cyclic loading conditions.[1] This type of fatigue failure occurs with maximum applied loads considerably lower than those which cause simple tensile or creep failure in a comparable interval of time and produce fracture morphologies which are very different from those found with other loading conditions. Under tensile or creep loading most synthetic fibers fail in a similar manner.[2] Crack growth is initiated at the fiber surface and develops in a radial direction into the fiber. The crack growth is initially stable and because of plastic deformation ahead of the crack it forms a diamond shaped wedge opening in the cylindrical fiber. Rapid failure eventually occurs when the crack has developed sufficiently into the fiber for the remaining cross section no longer to be able to support the applied stress. The two broken ends of the fiber have very similar appearances with an inclined surface corresponding to slow crack growth followed by a fracture zone normal to the fiber axis corresponding to rapid failure. Tensile fatigue failure is similarly initiated at the fiber surface but after crack propagation of only about 1 μm the crack is sharply deviated to run along the fiber at a slight angle to the fiber axis direction. The load bearing cross section is therefore gradually reduced until it finally fails by the simple tensile or creep failure process.[3]

The necessary loading criteria for fatigue failure are that the maximum cyclic load by sufficiently high, usually greater than 50% of the tensile

Journal of Applied Polymer Science, Vol. 29, 4363–4376 (1984)
 CCC 0021-8995/84/124363-14$04.00

breaking load and that the minimum be sufficiently low, near to zero load. The minimum load criterion has been found to differ with different fibers. The polyamide fiber in which the fatigue process was originally identified[3] required a zero miminim load, but subsequently other polyamide fibers of a different origin were found to fail with positive minimum loads of up to 4% of the tensile breaking load.[4] Raising the minimum load above this threshold, even if the cyclic load amplitude remained constant so that the maximum applied load increased, prevented failure.

Synthetic organic fibers are used extensively in structures in which they play a vital load bearing role. In the case where these structures are subjected to cyclic loading, tensile fatigue failure is a potentially important deterioration process. The structures of polyamide and polyester fibers have been widely discussed in the literature[5-9] and it is known that they are semicrystalline, consisting of blocks of well-ordered molecules surrounded by amorphous or randomly arranged molecules. The structures are anisotropic having a preferred molecular orientation parallel to the fiber axis due to the drawing process. The purpose of this study was to begin to explain in terms of structural modifications at the molecular level some of the observations of fatigue crack growth which have previously been reported.

Fiber Characteristics

The fibers which have been examined in this study were highly drawn PET multifilaments produced by Viscosuisse for use in tires, conveyor belts, etc. They were cylindrical with a smooth surface; the filament count was of 5.3 ($\pm$0.6) dtex and the filament diameter was 23.8 ($\pm$1.7) μm. A previous study using x-ray diffraction on bundles of multifilament continuous yarns of the same type revealed the structural parameters shown in Table I.[10]

EXPERIMENTAL

Tensile and Fatigue Tests

All of the mechanical tests on the fibers examined in this study were made on a Universal Fiber Tester, the details of which have been given elsewhere.[11] The apparatus allows tests to be made on single fine fibers with an accuracy of 0.1 g under tensile, creep, relaxation, and tensile fatigue conditions. The fiber is held between two jaws, one of which is attached to

TABLE I
Structural Data Obtained from a Number of Fibers[a]

X_c	k	X_s (%)	V_c (Å^3)	L_p (Å)	L_a (Å)
0.35	2.9	50.5	189×10^3	150	82

[a] X_c = crystallinity corrected according to the disorder factor; k = disorder factor[10]; X_s = percent crystallinity after Statton[14]; L_p = long period; L_a = length of amorphous zone parallel to the fiber axis; V_c = mean crystallite volume (from the broadening of the 2θ distributions of 100, 010, and $\bar{1}05$ lines.

a vibrator and the other to load cells. Under creep or fatigue conditions the required load level is assured through a servo-system which operates the traverse motor whenever the load on the fiber varies due to the nonelastic behavior of the material. The fatigue tests conducted in this study were all in the constant maximum load mode which, it has previously been shown, is preferable to other possible loading modes.[12] A sinusoidal loading pattern at 50 Hz was employed and tests were taken to failure or to 10^7 cycles, whichever was reached first. The specimen gauge length used was 50 mm.

Infrared Spectrometry

Several techniques were used in order to study the modifications of the fiber structure. Infrared spectrometry was used in order to obtain an estimation of the crystallinity and of the molecular orientation in the crystalline and amorphous zones. A Perkin-Elmer Spectrometer Model 112 with a single beam was used. The infrared covered the range from 2.5 to 12 μm (i.e., from 4000 to 835 cm^{-1}) and impinged on the fiber through a slit of 650 μm in the direction parallel to the fiber. The specimen was fixed with adhesive tape to a black slide fitted to the spectrometer stage and received no special preparation apart form drying in an air flow for 15 min before and during the recording of the spectrum.

Schmidt[13] has shown that the useful spectrum for PET is from 600 to 1100 cm^{-1} with an absorption band at 1580 cm^{-1}, which enables the orientation of the amorphous zones to be determined. The variations in crystallinity were revealed through changes in two parameters known as the trans index and the crystalline index.

The trans index I_t is a function of the crystalline zones plus aligned molecular chains not making up a crystallite. In the case of polarized incident light, it is defined as

$$I_t = \frac{2T_\perp + T^{/\!/}}{2R_\perp + R^{/\!/}}$$

where $T_\perp$ and $T^{/\!/}$ are the optical densities with the polarization respectively perpendicular and parallel to the fiber axis of the 973 cm^{-1} band and $R_\perp$ and $R^{/\!/}$ are the same parameters for a reference band at 793 cm^{-1}.

The crystalline index is a function only of the crystalline zones and is given by

$$I_c = \frac{2C_\perp + C^{/\!/}}{2R_\perp + R^{/\!/}}$$

where $C_\perp$ and $C^{/\!/}$ are the optical densities of the band at 845 cm^{-1}.

The molecular chain orientation is given by the dichroic ratio (i.e., $T^{/\!/}/T_\perp$) of the 875 cm^{-1} band, which characterizes the general orientation and the dichroic ratio of the 1580 cm^{-1} band for the orientation of the amorphous zones.

X-Ray Diffraction:

A semiquantitative analysis of crystallinity was made using x-ray diffraction. This technique has in the past been used to study bundles usually containing several 10 fibers.[14-16] In the course of the present study the technique was refined in order to study the structure of a single fiber in a precise zone. A lead screen, moveable in both the X and Y direction and pierced by a hole of 400 μm diameter, was positioned so as to perfectly align the x-ray beam and the fiber. The purpose of the hole was to limit the diameter of the beam. The volume of the diffracting material was therefore 1.8×10^{-13} m^3. The diffraction curve was recorded with a position sensitive linear detector (PSLD) coupled with a multichannel (512) analyzer. An exposure time of 2 h was judged sufficient with the 3 kW power generator, to obtain valid results; the background radiation was measured without a fiber in place and then automatically subtracted from the results obtained with a fiber with the aid of a microcomputer.

Transmission Electron Microscopy:

Transmission electron microscopy was used in order to study local modifications of the fiber structure particularly around the fatigue crack tip. The fiber was embedded in epoxy resin and then sliced with an ultramicrotome giving specimens with thicknesses of 500–1000 Å. The technique has been used extensively for the study of fibers[17-19] and has been described in detail in the literature.[20]

Section A–A in Figure 1 shows the form of the specimen obtained when the fiber was sliced near the crack tip at approximately 45° with respect to the axis. Section B–B shows a specimen prepared by slicing at a slight angle to the fiber axis and which enables the area just ahead of the crack tip to be studied. Electron diffraction studies have been made in the neighborhood of the crack tip. These proved difficult with normal beam intensities because of radiation-induced damage producing an amorphization of the structure.[21] The location of the diffracted areas studied was assured after the pattern was taken in low dose conditions, by irradiating these zones

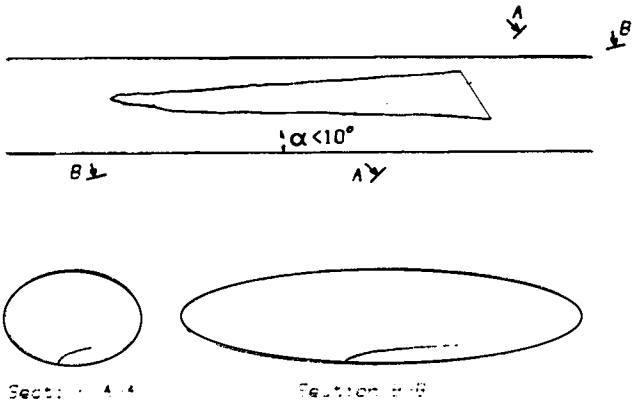

Fig. 1. Schematic representation of oblique transversal (A–A) and oblique longitudinal (B–B) section through the fatigue crack tip.

TABLE II
Mean Values of Loads, Stresses, and Strains at Failure during Simple Tensile Loading

Strain rate	Number of specimens	Failure load (g)	Stress (MPa)	Strain (%)
100%/mn	50	44.9 (±6.5)	980 (±96)	12.9 (±2.0)
60%/mn	100	45.0 (±7.0)	983 (±97)	13.5 (±2.5)
40%/mn	100	43.4 (±5.9)	965 (±89)	15.4 (±2.2)

with an intense electron beam which resulted in a clear area on the micrograph.

The diffracting area was a disk of about 0.5 μm diameter so that with a thickness of approximately 800 Å the diffracting volume was around 1.6 $\times$ 10^{-20} m^3 or 10^7 smaller than that studied by x-ray diffraction.

RESULTS

Tensile Tests and Fatigue Tests

Several series of simple tensile tests were conducted with different loading rates. Table II shows the results which were obtained and reveals that the breaking load did not change with loading rate but that the strain to failure decreased with increasing speed. Figure 2 shows the classical tensile type fracture morphology obtained after simple tensile loading.

Figure 3 shows that the fiber studied failed in fatigue as has been reported elsewhere. The crack growth along the fiber reduces the remaining cross section only very slowly as the angle of penetration is small compared with that observed for polyamide fibers. This results in a long fracture surface with final failure usually occurring behind the longitudinal crack front as the load supporting cross section fails in creep.

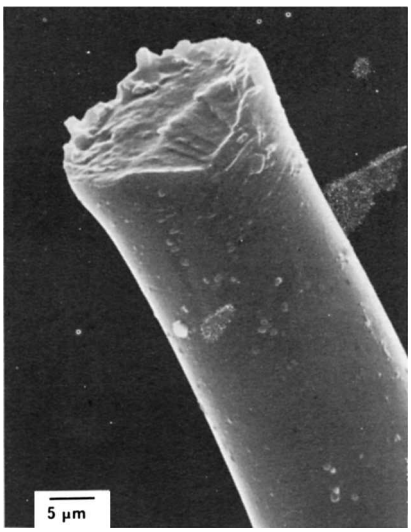

Fig. 2. Typical tensile fracture morphology of a PET fiber.

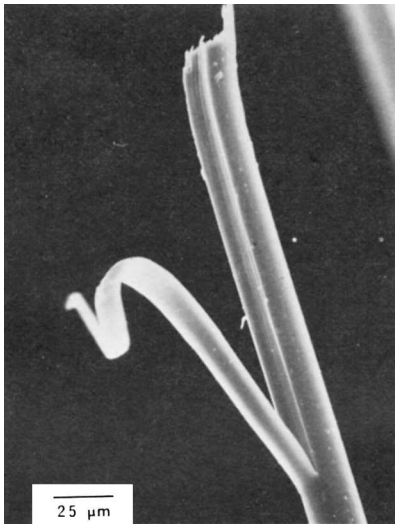

Fig. 3. Typical fatigue fracture morphology of a PET fiber.

Figure 4 shows the influence of the maximum applied load on the fiber fatigue lifetimes, with the minimum load being zero. It can be seen that the fatigue lifetimes reduce as the maximum load increases, with a particularly important difference between 60% and 65% of the simple breaking load.

The effect of the minimum load was studied with a maximum cyclic load of 70% of the tensile breaking load. Figure 5 shows that, although fatigue failure did occur with small positive minimum loads, a minimum load threshold did exist between 13% and 18% of the tensile breaking load. Several fatigue cracks were seen to coexist on some fibers as is shown in Figure 6.

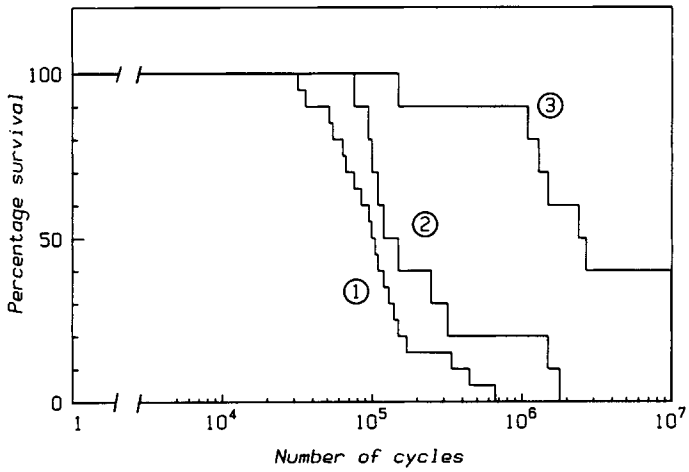

Fig. 4. Cumulative histograms of fatigue life times showing the influence of the maximum load: (1) maximum load 70% of tensile strength (R); (2) maximum load 65% R; (3) maximum load 60% R.

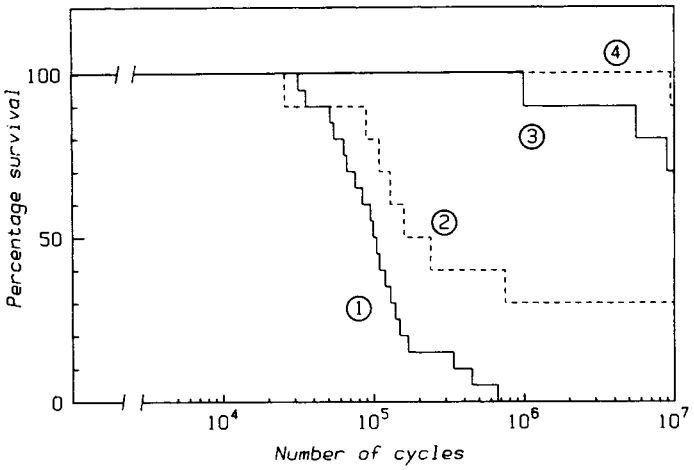

Fig. 5. Cumulative histograms of fatigue life times showing the influence of the minimum load with a maximum load = 70% R: (1) zero minimum load; (2) minimum load 6 g (13% R); (3) minimum load 8 g (18% R), (4) minimum load 10 g (22% R).

Failure due to creep processes can occur under cyclic loading, so constant load creep tests were conducted on the fibers. The failure histograms for fibers loaded to 90%, 80%, and 70% of their nominal breaking loads are shown in Figure 7. It can be seen that failure due to creep did not occur for loads equal to or less than 70% of the nominal breaking load in a time equivalent to 10^7 cycles. The fracture morphologies of fibers broken during creep tests were identical to those obtained in tensile tests.

Infrared Spectrometry

In order to examine the structure of the fibers during fatigue, the tests were stopped when a fatigue crack had developed but before failure of the

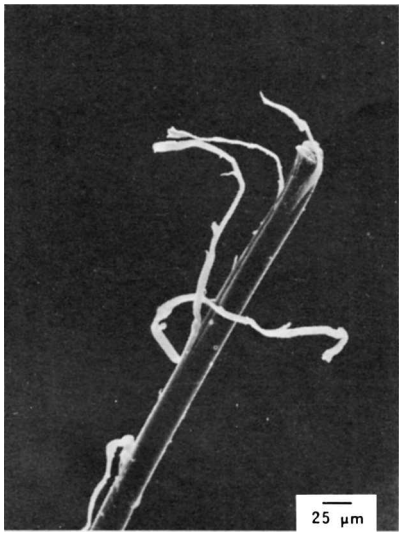

Fig. 6. Multiple fatigue fractures on a polyester fiber.

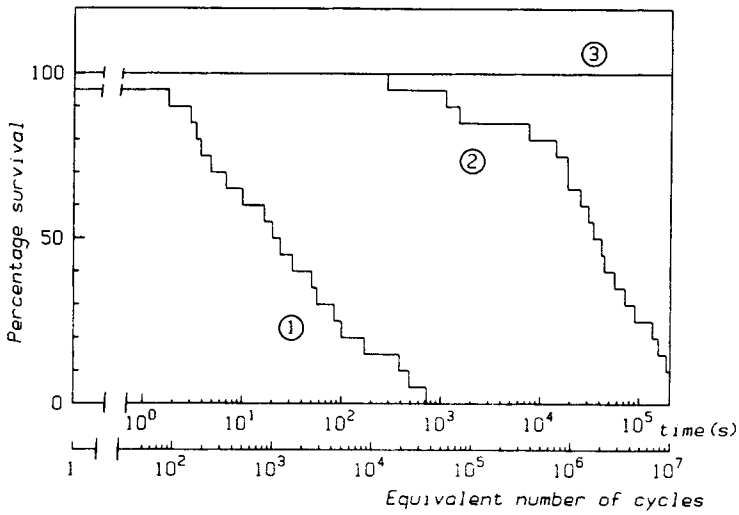

Fig. 7. Cumulative histograms of creep lifetimes: (1) 90% tensile strength (R); (2) 80% R; (3) 70% R.

fiber. The average number of cycles to arrive at this situation was 8×10^4 cycles. Comparative measurements were made with lengths of the filament neighboring the part which had been subjected to fatigue. In addition, cyclic tests were conducted under loading conditions which did not lead to fatigue cracking and these specimens examined after at least 8×10^4 cycles. These latter specimens will be referred to below as "control specimens." The results of these tests are shown in Table III which represent the average of 15 fibers tested for each loading condition. It is clear that a notable reduction of the parameters I_t and I_c corresponding to degree of crystallinity occurred

TABLE III
Infrared Spectrometry; Average Percentages of Crystallinity and Orientation Variation as a Function of Loading Mode

	Trans index I_t	Crystalline index I_c	General orientation $875\frac{\perp}{/\!/}$	Amorphous orientation $A\frac{/\!/}{\perp}$
Standard deviation (%)	± 7	± 8	±7	±13
Variation after cyclic loading inducing fatigue with a developing crack (%)	−20.4	−13.8	−1.4	− 2.1
Variation after cyclic loading which did not produce fatigue cracks (%)	− 6.7	+ 3.4	+6.3	− 3.8

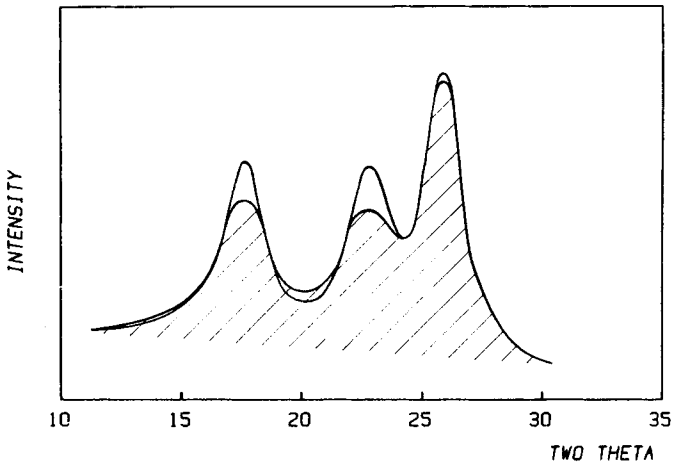

Fig. 8. Single fiber diffraction diagram obtained from the PSLD. The shaded curve is that obtained with a fatigued specimen and is superimposed on the curve obtained with an untested fiber.

under fatigue conditions whereas no such change was seen in the control specimens. No overall change in molecular orientation was observed with both types of specimen.

X-Ray Diffraction

Initial tests using x-ray diffraction were conducted on bundles of four fibers and revealed a fall in crystallinity during fatigue of 23%. Subsequently, the technique was improved so as to enable single fibers to be studied. Figure 8 shows an example of a diffraction diagram obtained with a single fiber. Averaging the values obtained with several fibers gave a reduction of crystallinity after fatigue of 20% whereas no change was found with the control specimens.

Transmission Electron Microscopy

Figure 9 shows an oblique transverse section of a fiber which contained a fatigue crack. Figure 10 shows the intensity curves derived from the electronic diffraction micrographs obtained at different places around the crack. It can be seen that the crystallinity in the zones near to the crack tip was greatly reduced.

Figures 11–13 show an oblique longitudinal section of a fiber which contained a fatigue crack. It can be seen that the crack was preceeded by a band of less dense material and that just ahead of the crack tip a series of micro voids were visible. Dark field micrographs obtained from the ($\bar{1}10$, 100) interference doublet isolated from the equatorial triplet revealed an absence of bright areas corresponding to crystallites and an accumulation of drawn out amorphous zones, particularly near the fatigue crack tip, as shown in Figure 14.

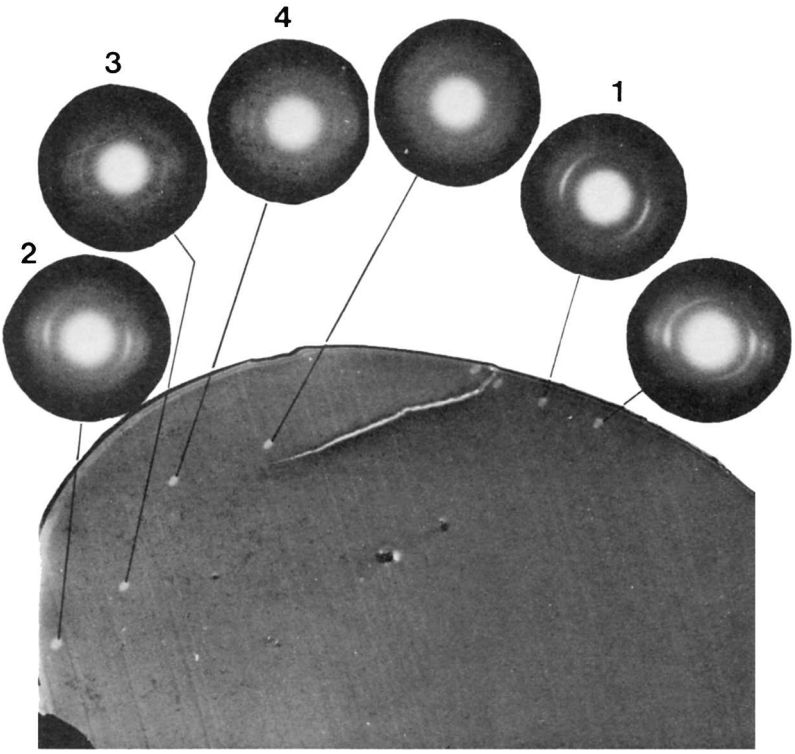

Fig. 9. Electron diffraction patterns obtained with a pseudotransversal section at the crack tip. The black outline corresponds to the gold–palladium deposit.

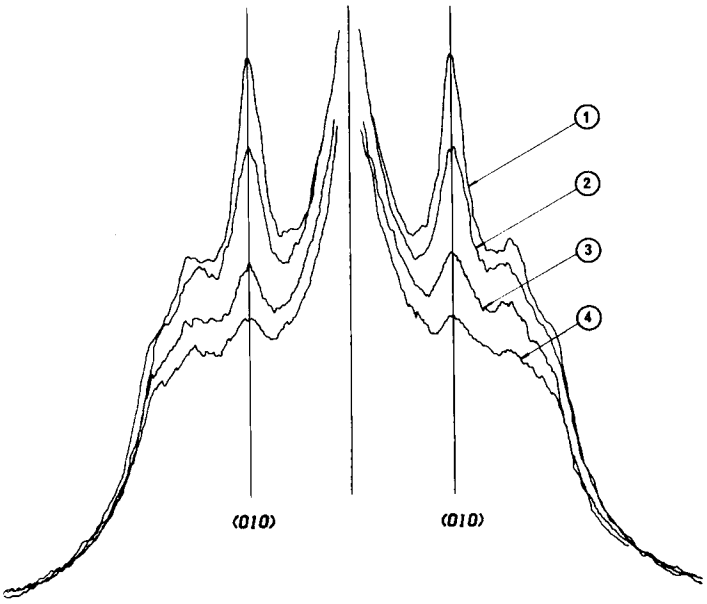

Fig. 10. Densiometric traces from electron diffraction patterns, nos. 1, 2, 3, 4 shown in Figure 9.

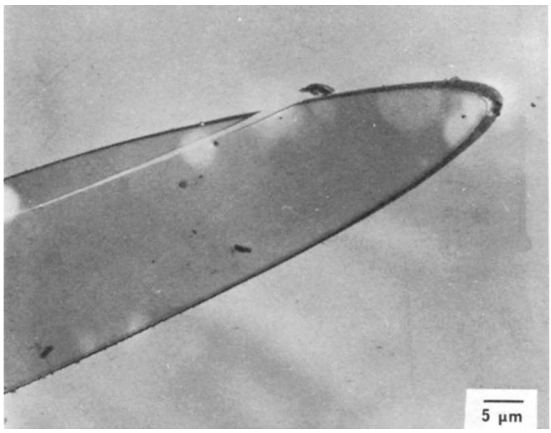

Fig. 11. Oblique longitudinal section of a PET fiber containing a fatigue crack.

DISCUSSION

This present study has confirmed the existence of a tensile fatigue process in polyester fibers which results in a distinct fracture morphology. The fatigue crack growth along the polyester fiber is generally much longer than that found with polyamide fibers. Failure of the fiber finally occurs when the load bearing cross section is sufficiently reduced for simple tensile or creep crack growth to occur. The final point of rupture of polyester fibers is often seen to be some way behind the fatigue crack tip. This is not usually the case with polyamide fibers and suggests that, while simple tensile failure breaks the reduced load bearing section in the latter fibers, it is the creep process which dominates the final stage of the fatigue failure of polyester.

The fibers tested in this study failed by fatigue even when the minimum applied load was positive; however, the minimum load was seen to be very significant. A threshold level for the minimum load determined to be between 13 and 18% of the nominal breaking load, above which fatigue failure

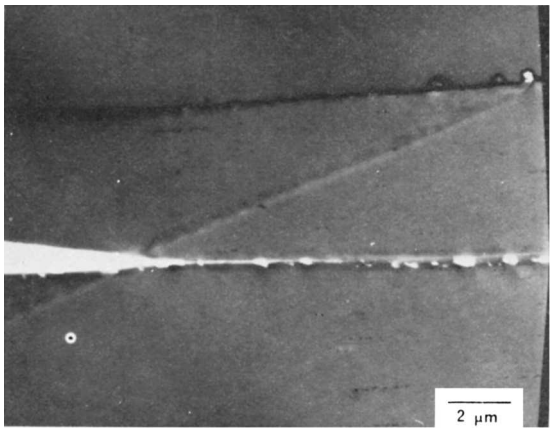

Fig. 12. Detail of crack tip preceeded by micropores.

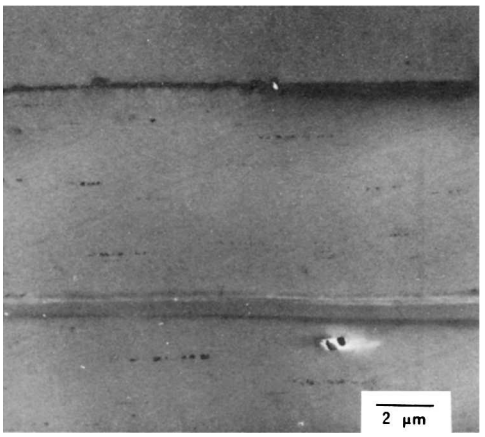

Fig. 13. Detail of the zone of the fatigue crack showing an amorphous band.

was found not to occur within 10^7 cycles. The same type of behavior has been observed with polyamide fibers.[4] The processes which govern the minimum load criterion for fatigue failure are not known, but, as the threshold level is different for fibers of different types, or obtained from different sources, the criterion may be due to the internal stress state of the fiber caused by its thermal and chemical history. The industrial treatments to which the fibers of this study were subjected are not known.

Infrared spectroscopy has revealed a fall in crystallinity in fibers subjected to cyclic loading conditions which lead to fatigue failure. No such change was observed in "control" fibers subjected to cyclic loading which did not produce fatigue. This observation was confirmed by x-ray diffraction. No changes in overall structural orientation were measured after cyclic loading. Observations made by transmission electron microscopy and electron diffraction have revealed that an amorphous band is created in the fiber under fatigue loading conditions. The fatigue crack propagates along this band and is preceeded just ahead of the crack tip by the creation of small voids. The crack propagates most probably by joining up these voids. It is probable that the elongated amorphous areas observed by dark field electron microscopy precede the creation of the band which is formed by their coalescing. The creation of the amorphous band therefore seems likely to occur by the breaking up and movement of the crystalline blocks rather than their melting as there seems not to be enough energy available for this latter process. If this is the case the density of the amorphous zones may play a crucial role governing the development of fatigue cracks.

CONCLUSION

Polyester fibers fail by a fatigue process under certain cyclic tensile loading conditions. When tensile fatigue failure occurs, it results in an unmistakable fiber fracture morphology. Criteria for such a fatigue failure are a sufficiently high maximum load and a sufficiently low minimum load. Fatigue failure is accompanied by a fall in crystallinity. Amorphous zones are created in the fiber which coalesce into a band along which the fatigue

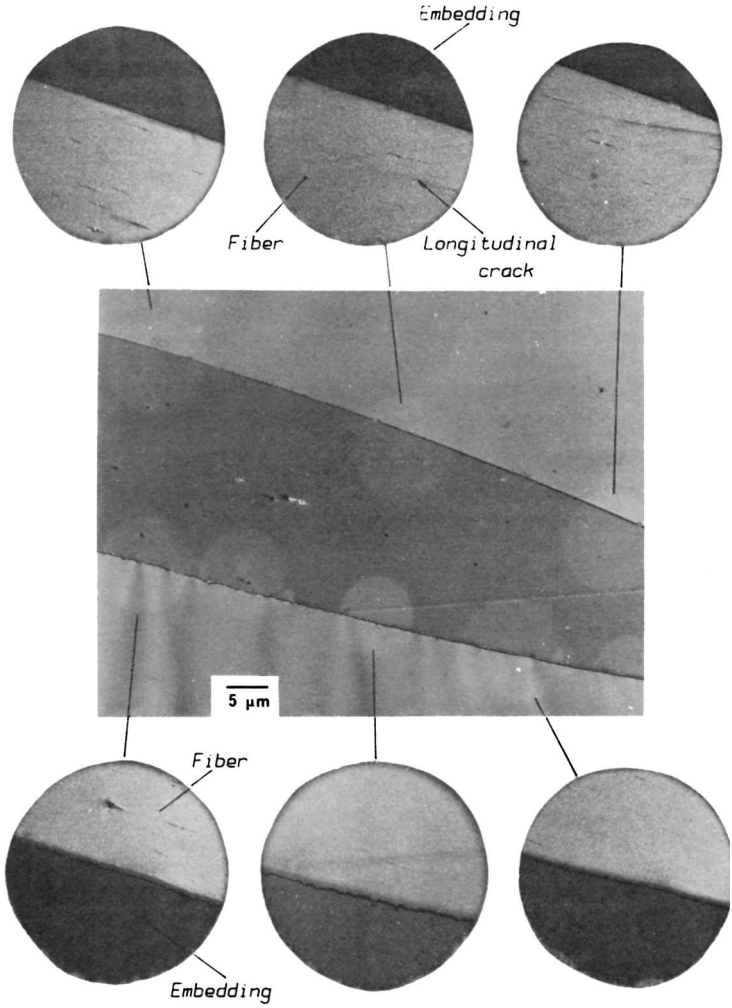

Fig. 14. Dark field micrographs obtained from oblique longitudinal section of a fibre containing a fatigue crack; the crack is indicated by an arrow; an accumulation of elongated amorphous zones (black regions) ahead of the crack should be noticed.

crack propagates. The crack grows by joining up small voids which are created just ahead of the fatigue crack tip.

References

1. A. R. Bunsell and J. W. S. Hearle, *J. Appl. Polym. Sci.*, **18**, 267 (1974).
2. J. W. S. Hearle and E. A. Vaughn, *Rheol. Acta*, **9**(1), 76 (1970).
3. A. R. Bunsell and J. W. S. Hearle, *J. Mater. Sci.*, **6**, 1303 (1971).
4. Ch. Oudet and A. R. Bunsell, *J. Mater. Sci. Lett.*, to appear.
5. J. W. S. Hearle and R. Greer, *Text. Prog.*, **2**(4), 203 (1970).
6. A. Peterlin, *Text. Res. J.*, **42**, 20 (1972).
7. R. Meredith, *Text. Prog.*, **7**(4), 74 (1975).
8. D. C. Prevorsek and Y. D. Kwon, *J. Macromol. Sci. Phys.*, **B12**(4), 447 (1976).
9. C. Hinrichsen, *Melliand Textilberichte*, **1**, 7 (1977).

10. M. Sotton, *A. C. S. Symposium Series*, **141**, 193–213 (1979).
11. A. R. Bunsell, J. W. S. Hearle, and R. D. Hunter, *J. Phys. E: Sci. Instrum.*, **4**, 868 (1971).
12. J. W. S. Hearle, *J. Mater. Sci.*, **2**, 474 (1967).
13. P. G. Schmidt, *J. Polym. Sci., Part A*, **1**, 1271 (1963).
14. W. O. Statton, *J. Appl. Polym. Sci.*, **7**, 803 (1963).
15. J. H. Dumbleton, *J. Appl. Polym. Sci.*, **A2**, 2067 (1968).
16. D. C. Prevorsek, *J. Polym. Sci. Symp.*, **32**, 343 (1971).
17. A. C. Reimschuessel and D. C. Prevorsek, *J. Polym. Sci.*, **14**, 485 (1976).
18. S. C. Bennett and D. J. Johnson, *Carbon*, Pergamon, New York, 1979, Vol. 17, pp. 25.
19. D. J. Johnson, *Phil. Trans. Roy. Soc. Lond. A*, **294**, 443 (1980).
20. R. Hagege and J. Hagege, *Technique de Laboratoire*, Masson, Paris, 1980, Vol. 4, pp. 123.
21. R. Hagege, *A. C. S. Symposium Series*, **141**, 280–301 (1979).

Received April 10, 1984
Accepted May 7, 1984